Journal of Plant Physiology 232 (2019) 248–256

Contents lists available at ScienceDirect

Journal of Plant Physiology

journal homepage: www.elsevier.com/locate/jplph

# Orchestration of Cu-Zn SOD and class III peroxidase with upstream interplay between NADPH oxidase and PM $H^+$-ATPase mediates root growth in *Vigna radiata* (L.) Wilczek

Arkajo Majumdar[a,b], Rup Kumar Kar[a,*]

[a] Plant Physiology and Biochemistry Laboratory, Department of Botany, Visva-Bharati University, Santiniketan, 731235, West Bengal, India
[b] Department of Botany, City College, 102/1 Raja Rammohan Sarani, Kolkata, 700009, West Bengal, India

ARTICLE INFO

*Keywords:*
Calcium ($Ca^{+2}$)
Class III peroxidase
NADPH oxidase
Plasma membrane $H^+$-ATPase
Root growth
Superoxide dismutase

ABSTRACT

Post-germination plant growth depends on the regulation of reactive oxygen species (ROS) metabolism, spatiotemporal pH changes and $Ca^{+2}$ homeostasis, whose potential integration has been studied during *Vigna radiata* (L.) Wilczek root growth. The dissipation of proton ($H^+$) gradients across plasma membrane (PM) by CCCP (protonophore) and the inhibition of PM $H^+$-ATPase by sodium orthovanadate repressed SOD (superoxide dismutase; EC 1.15.1.1) activity as revealed by spectrophotometric and native PAGE assay results. Similar results derived from treatment with DPI (NADPH oxidase inhibitor) and Tiron ($O_2^{\cdot-}$ scavenger) denote a functional synchronization of SOD, PM $H^+$-ATPase and NOX, as the latter two enzymes are substrate sources for SOD ($H^+$ and $O_2^{\cdot-}$, respectively) and are involved in a feed-forward loop. After SOD inactivation, a decline in apoplastic $H_2O_2$ content was observed in each treatment group, emerging as a possible cause of the diminution of class III peroxidase (Prx; EC 1.11.1.7), which utilizes $H_2O_2$ as a substrate. In agreement with the pivotal role of $Ca^{+2}$ in PM $H^+$-ATPase and NOX activation, $Ca^{+2}$ homeostasis antagonists, i.e., $LaCl_3$ ($Ca^{+2}$ channel inhibitor), EGTA ($Ca^{+2}$ chelator) and LiCl (endosomal $Ca^{+2}$ release blocker), inhibited both SOD and Prx. Finally, a drastic reduction in apoplastic $^{\cdot}OH$ (hydroxyl radical) concentrations (induced by each treatment, leading to Prx inhibition) was observed via fluorometric analysis. A consequential inhibition of root growth observed under each treatment denotes the importance of the orchestrated functioning of PM $H^+$-ATPase, NOX, Cu-Zn SOD and Prx during root growth. A working model demonstrating postulated enzymatic synchronization with an intervening role of $Ca^{+2}$ is proposed.

## 1. Introduction

A plethora of research conducted over the last few decades has strongly established the role of reactive oxygen species (ROS) in plant growth and development (Müller et al., 2009; Causin et al., 2012; Tsukagoshi, 2016; Černý et al., 2018). Although the distribution of ROS generators throughout the plant body corroborates the importance of ROS-mediation in diverse plant processes, these generators are strictly site-specific (Kar, 2015). Roots that are completely skotomorphogenic in nature lack chloroplast-derived ROS, a major portion of cellular ROS found in leaves. Rather, plasma membrane (PM)-located NADPH oxidases [NOXs; or respiratory burst oxidase homologues (RBOHs)], in addition to other minor sources, are primarily tasked with producing ROS (superoxide, $O_2^{\cdot-}$) via the one electron-reduction of $O_2$ in apoplastic space, which is necessary for root growth (Foreman et al., 2003; Dunand et al., 2007; Fluhr, 2009). Superoxide produced from NOX activity is converted either enzymatically (by apoplastic SOD) or spontaneously into different suitable forms which are then utilized for various purposes, *viz.* cell wall loosening (by $^{\cdot}OH$; Airianah et al., 2016) and stiffening (by $H_2O_2$; Schopfer, 1996).

Superoxide dismutases (SODs; EC 1.15.1.1) are the primary enzymes responsible for the dismutation of $O_2^{\cdot-}$ to $H_2O_2$ at various subcellular locations e.g., chloroplast, mitochondria, peroxisome and apoplastic space (Alscher et al., 2002; Woith et al., 2017; Černý et al.,

*Abbreviations:* CCCP, carbonyl cyanide chlorophenylhydrazone; DEDTC, N,N-diethyldithiocarbamate; DMTU, 1,3-dimethyl-2-thiourea; DPI, diphenylene-iodonium chloride; DTT, dithiothreitol; EDTA, ethylenediaminetetraacetic acid; EGTA, ethylene glycol bis (2-aminoethyl *N,N,N′,N′*-tetra acetic acid; NBT, nitroblue tetrazolium chloride; PVP, polyvinylpyrrolidone; ROS, Reactive oxygen species; Tiron, sodium 4,5-dihydroxybenzene-1,3-disulfonate; XTT, 2,3-Bis(2-methoxy-4-nitro-5-sulfophenyl)-2H-tetrazolium-5-carboxanilide inner salt

* Corresponding author.
*E-mail address:* rupkumar.kar@visva-bharati.ac.in (R.K. Kar).

https://doi.org/10.1016/j.jplph.2018.11.001
Received 15 August 2018; Received in revised form 1 November 2018; Accepted 2 November 2018
Available online 08 November 2018
0176-1617/ 

2018). Generally, SODs are regarded as a first line of defence against different stresses e.g., osmotic (Naderi et al., 2014) and drought (Abedi and Pakniyat, 2010), when rapid $O_2^{\cdot-}$ elimination is required. However, the involvement of SODs in growth has been identified over time, as accumulating evidence supports a pivotal role of $H_2O_2$ in plant growth and development (Ogawa et al., 1997; Singh et al., 2016; Li et al., 2017). Depending on the metal cofactors involved, SODs are classified into separate groups, *viz.* Fe-SOD, Mn-SOD, Cu-Zn SOD and Ni-SOD (Alscher et al., 2002; Miller, 2004). Among these groups, apoplastic Cu-Zn SOD is crucial for root growth because it is predominantly responsible for converting NOX-generated apoplastic $O_2^{\cdot-}$ into $H_2O_2$. However, according to the basic two-step disproportionation reaction of SODs, i.e., $2\ O_2^{\cdot-} + 2\ H^+ \leftrightarrow O_2 + H_2O_2$ (Miller, 2003, 2004), the availability of protons ($H^+$) in the apoplast appears to be equally essential for Cu-Zn SOD to convert apoplastic $O_2^{\cdot-}$ into $H_2O_2$. Besides its involvement in maintaining membrane potential, in synchrony with NOX, by charge compensation through regulated $H^+$ extrusion (Majumdar and Kar, 2018) and other acidification mediated growth processes, e.g., the promotion of expansin (Hager, 2003), PM $H^+$-ATPase can also be considered a candidate enzyme that provides a steady supply of $H^+$ required for Cu-Zn SOD activity in the apoplast during root growth. Therefore, the existence of a positive functional correlation among the three enzymes i.e., SOD, NOX and PM $H^+$-ATPase, seems justifiable, as the latter two provide substrates for SOD ($O_2^{\cdot-}$ and $H^+$, respectively). However, no report on this issue is available to date, leaving the possibility unexplored.

As housekeeping enzymes, heme-containing class III peroxidases (Prx; EC 1.11.1.7) have been studied extensively and shown to be deeply involved in plant defence mechanisms (Penel et al., 1992; Almagro et al., 2009) and growth processes (Dunand et al., 2007; Francoz et al., 2015; Moural et al., 2017). Apart from their peroxidative cycle, which produces free radicals that form covalent linkages and lead to cell wall stiffening (Passardi et al., 2005), Prxs produce $^{\cdot}OH$ radicals (the most reactive ROS form) via the hydroxylic cycle using $H_2O_2$ as a substrate (Chen and Schopfer, 1999; Cosio and Dunand, 2009; Raggi et al., 2015). This $^{\cdot}OH$ radical nonenzymatically cleaves cell wall polysaccharides and causes wall loosening, thus effectively enhancing the plastic extensibility of the cell wall (Schopfer, 2001; Liszkay et al., 2004; Cosio and Dunand, 2009). As the production of $H_2O_2$ in roots seems to be regulated by the coordinated activities of SOD, NOX and PM $H^+$-ATPase, the involvement of Prxs in the described functional enzymatic synchronization process is possible. Intracellular $Ca^{+2}$ homeostasis plays a pivotal role in numerous plant processes and, most importantly, involves the orchestration of complex cellular signals (Siddiqui et al., 2012). Furthetmore, $Ca^{+2}$ (a prime second messenger) differentially regulates NOX, PM $H^+$-ATPase and Prx activity (Sagi and Fluhr, 2006; Janicka-Russak, 2011; Pintus et al., 2011; Gilroy et al., 2014; Singh et al., 2015; Majumdar and Kar, 2018) and can serve as a link between enzymes.

A positive feed-forward loop between NOX and PM $H^+$-ATPase has been identified (Majumdar and Kar, 2018), demonstrating the reciprocal regulation of these two enzymes. As these two enzymes provide the substrates in apoplastic space for downstream enzymes, SOD and, in turn, Prx (which are actively involved in cell wall relaxation), the present investigation attempts to recognize and comprehend the plausible functional correlation of SOD and Prx with upstream interplay between PM $H^+$-ATPase and NOX in relation to root growth using *Vigna radiata* (L.) Wilczek as a model system. The potent role of $Ca^{+2}$ in mediating harmony is examined and a working model elucidating the relationship between the enzymes is proposed.

## 2. Materials and methods

### 2.1. Plant material

Mung bean [*Vigna radiata* (L.) Wilczek var B1] seeds were collected from the Pulses and Oilseeds Research Station in Berhampur, West Bengal, India. Seeds were first surface sterilized in 0.1% sodium hypochlorite solution, rinsed with distilled water several times, and then germinated on moistened (with distilled water) Whatman No. 1 filter paper in Petri dishes for 12 h. The germinated seeds were transferred to and incubated in respective test solutions (as described below) for 48 h in continuous darkness. Both the germination and incubation processes were maintained at a temperature of 30 ± 2 °C in a seed germinator. Root portions of the seedlings grown for 48 h were used for experiments.

### 2.2. Pharmacological treatments

To assess the role of the studied enzymes in root growth, germinated seeds were incubated in the following test solutions for pharmacological treatment: sodium orthovanadate (100 μM; specific P-type ATPase inhibitor), CCCP (50 μM; protonophore), DPI (20 μM; NOX inhibitor), Tiron (1 mM; superoxide scavenger), DMTU (1 mM; $H_2O_2$ scavenger), DEDTC (1 mM; SOD inhibitor), $LaCl_3$ (100 μM; $Ca^{+2}$ channel blocker), EGTA (100 μM; $Ca^{+2}$ chelator) and LiCl (2 mM; endosomal $Ca^{+2}$ release blocker). Apart from these, $H_2O_2$ was used at concentrations of 25 μM to 1 mM.

### 2.3. Growth parameters

Comparative growth studies were carried out by measuring the lengths and fresh weights of 10 roots (of seedlings grown for 2 days) from each treatment set, including a control; each experimental condition was replicated 3 times.

### 2.4. Spectrophotometric estimation of apoplastic superoxide

Apoplastic superoxide was estimated by a XTT reduction assay according to Majumdar and Kar (2018). Excised roots (300 mg) were incubated in 1 mL of K-phosphate buffer (20 mM, pH 6.0) containing XTT (500 μM) in complete darkness on a shaker for 45 min at room temperature. After incubation, the absorbance of the bathing medium was measured at 470 nm using a UV–vis spectrophotometer (Systronics, India). The molar concentration of $O_2^-$ (calculated from $A_{470}$ by using a molar extinction coefficient of $2.16 \times 10^4$ L $mol^{-1}$ $cm^{-1}$) was estimated for individual treatments. Wound-induced superoxide development was prevented by storing excised roots in distilled water for 10 min.

### 2.5. Spectrophotometric estimation of apoplastic $H_2O_2$

Apoplastic $H_2O_2$ content was measured spectrophotometrically according to Gay and Gebicki (2000), Minibayeva et al. (2009) and Moothoo-Padayachie et al. (2016). Three replicates with equal amounts (300 mg) of excised root tissue from each treatment group were immersed in 1.5 mL of bathing medium consisting of 1 part Reagent A and 100 parts Reagent B and gently shaken at 60 rpm for 30 min at 25 °C in the dark. Reagent A was composed of $FeSO_4$ (25 mM), $(NH_4)_2SO_4$ (25 mM) and $H_2SO_4$ (2.5 M), and Reagent B contained Xylenol orange (125 μM) and sorbitol (100 mM). After incubation, the absorbance of the assay mixture was measured at 560 nm. $H_2O_2$ production was calculated from a standard curve prepared from known concentrations of $H_2O_2$ and was represented as pmol $H_2O_2$-produced $g^{-1}$ FW $min^{-1}$.

### 2.6. Spectrofluorometric assay of apoplastic OH radical

Apoplastic OH radical content was measured according to Schopfer et al. (2001) with modifications. Excised root tissue (400 mg) was incubated in 3.0 mL of K-phosphate buffer (50 mM, pH 5.8) containing Na-benzoate (2.5 mM) for 6 h in the dark on a cyclomixer (REMI CM–101). After incubation, the bathing medium was centrifuged at

5000 rpm for 10 min at 25 °C, and fluorescence (excitation: 305 nm; emission: 407 nm) was measured using a fluorescence spectrophotometer. Blanks (without benzoate) were run in parallel to negate any unspecific fluorescence.

### 2.7. Spectrophotometric assay of SOD

A spectrophotometric assay of SOD was performed using a photochemical NBT reduction assay according to Giannopolitis and Ries (1977) with modifications. Root tissue (300 mg) was extracted in 1.5 mL of K-phosphate buffer (100 mM, pH 7.8) containing EDTA (0.1 mM) and centrifuged at 12,000 rpm for 20 min at 4 °C. The supernatant was used as the crude enzyme sample. The reaction mixture included 1 mL each of enzyme extract, $Na_2CO_3$ (final concentration of 50 mM), methionine (final concentration 13 mM), riboflavin (final concentration of 1.3 μM) and NBT (final concentration of 63 μM). The mixture was shaken well and incubated in glass test tubes under a white fluorescent lamp at 200 μmol $m^{-2}$ $s^{-1}$ for 30 min at 25 °C. Blank samples were composed of identical solutions and incubated in the dark. After incubation, the absorbance of the reaction mixtures and blanks was measured at 560 nm. SOD activity was measured in U $min^{-1}$ $mg^{-1}$ protein according to Woith et al. (2017).

### 2.8. Spectrophotometric assay of Prx

Prx activity was determined spectrophotometrically according to the method provided by Singh et al. (2015) with modifications. Root tissue (300 mg) was homogenized in 1.5 mL of phosphate-citrate buffer (50 mM, pH 6.0) and centrifuged at 7000 rpm for 15 min at 4 °C, and the supernatant was used as a crude enzyme sample. Next, 200 μL of phosphate buffer (50 mM, pH 6.8), 200 μL of $H_2O_2$ (10 mM) and 200 μL of pyrogallol (10 mM) were added to 200 μL of the enzyme sample, and the mixture was incubated for 2 min at 25 °C. The reaction was stopped by the addition of 200 μL of $H_2SO_4$ (5%). For every treatment, respective inactive sets were prepared via killing the enzyme by adding $H_2SO_4$ prior to incubation. The amount of pyrogallol oxidized was determined by measuring the absorbance (of purpurogallin) at 430 nm. Enzyme activity was measured according to Fick and Qualset (1975) using the formula [ΔA × T] / [t × v × w], where Δ*A* is the corrected absorbance ($A_{active} - A_{inactive}$), *T* is the total volume of the enzyme extract, *t* is the time of incubation, *v* is the enzyme volume during the reaction and *w* is the total weight of the tissue taken. Enzyme activity is expressed as enzyme units $min^{-1}$ $g^{-1}$ fresh weight (U $min^{-1}$ $g^{-1}$ FW).

### 2.9. Native PAGE assay of SOD

An in-gel assay of SOD was performed according to the method provided by Chen and Pan (1996) with modifications. Root tissue (300 mg) was extracted with 1.5 mL of Tris-HCl buffer (150 mM, pH 7.5) under chilled conditions and centrifuged at 12,000 rpm for 15 min at 4 °C. The supernatant was used as a crude enzyme sample and 30 μg of protein was subjected to native PAGE (10% non-denaturing resolving gel with a 5% stacking gel). The gels were stained according to the method provided by Beauchamp and Fridovich (1971). After electrophoresis, the gel slabs were immersed in 25 mL of NBT (1.23 mM), incubated in the dark for 15 min and briefly rinsed in distilled water. The gel was then immersed in 25 mL of K-phosphate buffer (100 mM, pH 7.0) containing TEMED (28 mM) and riboflavin ($2.8 \times 10^{-2}$ M) for another 15 min. The gel was quickly rinsed again and illuminated at a light intensity of 200 μmol $m^{-2}$ $s^{-1}$ for 15 min to initiate photochemical reactions. SOD activity was measured as white achromatic bands appearing against a blue-violet background. Different isoforms of SOD were identified via an inhibition test using $H_2O_2$ (10 mM) and KCN (5 mM). Image analysis and quantification were executed with ImageJ (Rivoal et al., 2002), a public domain programe available at http://rsb.info.nih.gov/ij/.

### 2.10. Native PAGE assay of Prx

An in-gel assay of Prx was performed according to the method provided by Prodanovic et al. (2007) with modifications. Root tissue (300 mg) was extracted with 1.5 mL of Tris-HCl buffer (100 mM, pH 7.5) containing DTT (1 mM), EDTA (1 mM) and PVP (2%) and centrifuged at 7000 rpm for 15 min at 4 °C. The supernatant was used for an in-gel assay of Prx activity and 25 μg of protein was subjected to native PAGE (7.5% nondenaturing resolving gel with a 5% stacking gel). The gel-slabs were stained with sodium-acetate buffer (50 mM, pH 5.5) containing 3,3′-diaminobenzidine (DAB, 0.1%) and $H_2O_2$ (5 mM). Brown-coloured bands corresponding to Prx activity appeared. Image analysis and quantification were conducted with ImageJ.

### 2.11. Statistical analysis

Data are presented with standard errors (SEs) of means, shown as vertical bars in the figures. Data were analysed via an appropriate single-factor ANOVA, and post hoc comparisons were drawn using Tukey's HSD to determine statistically significant differences among individual treatments at the $P < 0.05$ level according to Singh et al. (2015).

## 3. Results

### 3.1. Effects of vanadate and CCCP on SOD and Prx

Root growth was severely inhibited by sodium orthovanadate and CCCP (Fig. S1). Both agents individually restricted root growth at 50% of the control (distilled water) in terms of root lengths and fresh weights (Fig. S1a and b). A significant decline in apoplastic $H_2O_2$ generation under both treatments was observed in the roots of *V. radiata*. Thus, $H_2O_2$ was produced at rates of 186.53 pmol $g^{-1}$ FW $min^{-1}$ and 157.1 pmol $g^{-1}$ FW $min^{-1}$ under the CCCP and vanadate treatments, respectively, relative to the control (299.13 pmol $g^{-1}$ FW $min^{-1}$) (Fig. 1a). The involvement of PM $H^+$-ATPase activity and a stable cross PM proton gradient in the regulation of SOD was evident under vanadate and CCCP treatments. Thus, a significant inhibition of SOD activity was observed via the spectrophotometric analysis, as lower values were observed for the vanadate (0.099 U $min^{-1}$ $mg^{-1}$ protein) and CCCP (0.106 U $min^{-1}$ $mg^{-1}$ protein) treatments than with the control (0.122 U $min^{-1}$ $mg^{-1}$ protein) (Fig. 1b). This result was further corroborated by an in-gel native PAGE assay, which demonstrated a sharp decline in SOD activity. Achromatic bands were much weaker for lanes corresponding to treatments than for the control lane (Fig. 1c). Similarly, both vanadate and CCCP suppressed Prx activity. Spectrophotometric assay results showed a drastic inhibition of Prx under vanadate (40.62 U $min^{-1}$ $g^{-1}$ FW) and CCCP (50.4 U $min^{-1}$ $g^{-1}$ FW) treatment relative to that in the control (59.86 U $min^{-1}$ $g^{-1}$ FW) (Fig. 1d). Native PAGE results further confirmed the presence of reduced Prx activity under both treatments, as of treatment lane bands were distinctly weaker than control lane bands (Fig. 1e).

### 3.2. Effects of superoxide scavengers and $H_2O_2$ on SOD

DPI and Tiron treatment results demonstrated that the concentration of available superoxide determined the SOD functioning rate (Fig. 2). SOD activity, determined spectrophotometrically from the root extract, decreased considerably in response to DPI (0.065 U $min^{-1}$ $mg^{-1}$ protein) and Tiron (0.079 U $min^{-1}$ $mg^{-1}$ protein) treatments relative to that observed in the control (0.107 U $min^{-1}$ $mg^{-1}$ protein) (Fig. 2a). In-gel assay results also support this observation, as the treatment lanes showed decreased enzyme activity in terms of band intensity relative to that in the control lane (Fig. 2b). Interestingly, the inclusion of different concentrations of exogenous $H_2O_2$ in the incubation medium had dose-dependent effects on SOD. Thus enhanced

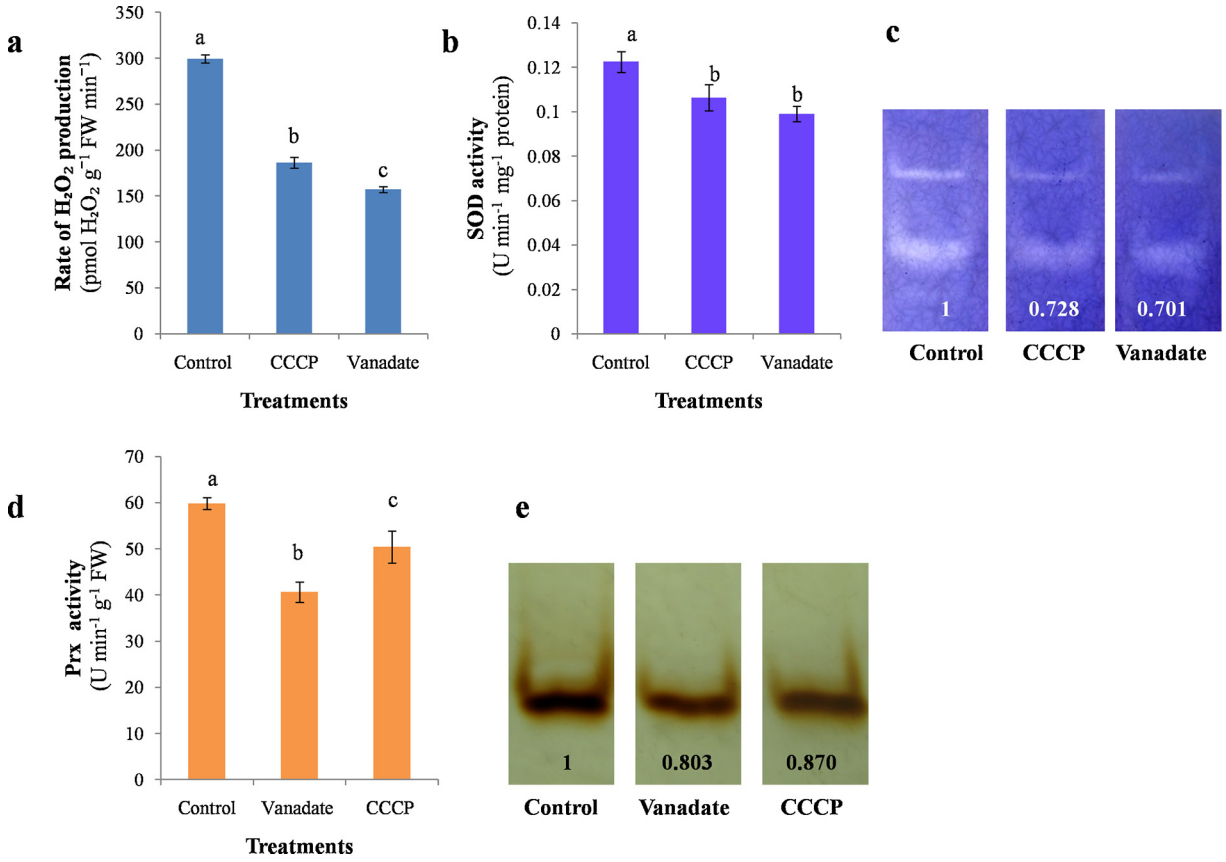


**Fig. 1.** Evaluation of the role of PM $H^+$-ATPase (and proton extrusion) in ROS homeostasis. **(a)** Xylenol orange assay of apoplastic $H_2O_2$ production by roots of seedlings incubated in vanadate (100 µM) and CCCP (50 µM) for 2 days along with control values. **(b)** SOD activity measured spectrophotometrically from total cellular extracts of roots incubated in vanadate (100 µM) and CCCP (50 µM) along with control values ($n = 3$; $F = 27.46$; $p < 0.05$). **(c)** *In-gel* native PAGE assay of SOD using NBT showing differential effects of vanadate (100 µM) and CCCP (50 µM) relative to control values as white achromatic bands. Numeric values denote relative band intensity levels. **(d)** Effects of vanadate (100 µM) and CCCP (50 µM) on Prx activity as determined by a spectrophotometric assay ($n = 3$; $F = 25.39$; $p < 0.05$). **(e)** *In-gel* native PAGE assay of Prx using DAB demonstrating the inhibitory effects of vanadate (100 µM) and CCCP (50 µM) relative to the control, shown as brown bands. Numeric values denote relative band intensity.

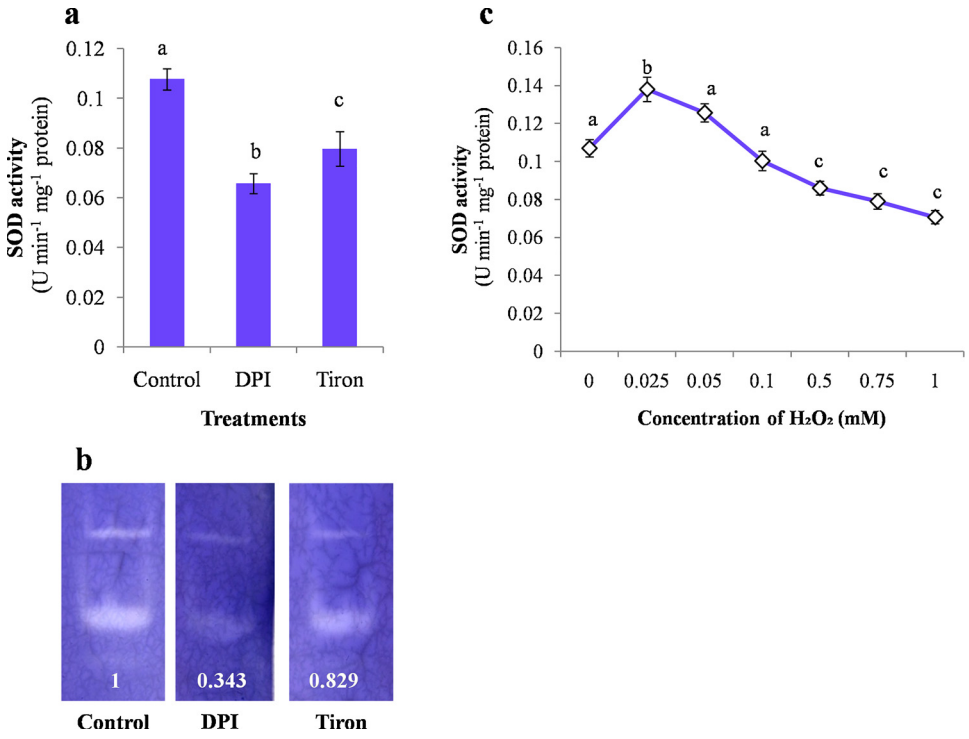


**Fig. 2.** Assay of SOD activity after treatment with a ROS scavenger, ROS enzyme inhibitor and different concentrations of $H_2O_2$. **(a)** SOD activity measured spectrophotometrically in total cellular extracts of roots incubated in DPI (20 µM) and Tiron (1 mM) along with control values ($n = 3$; $F = 6.28$; $p < 0.05$). **(b)** *In-gel* native PAGE assay of SOD using NBT showing the differential effects of DPI (20 µM) and Tiron (1 mM) relative to the control, shown as white achromatic bands. Numeric values denote relative band intensity levels. **(c)** Modulation of SOD activity by different concentrations of exogenous $H_2O_2$ as determination by a spectrophotometric assay ($n = 3$; $F = 44.72$; $p < 0.05$).

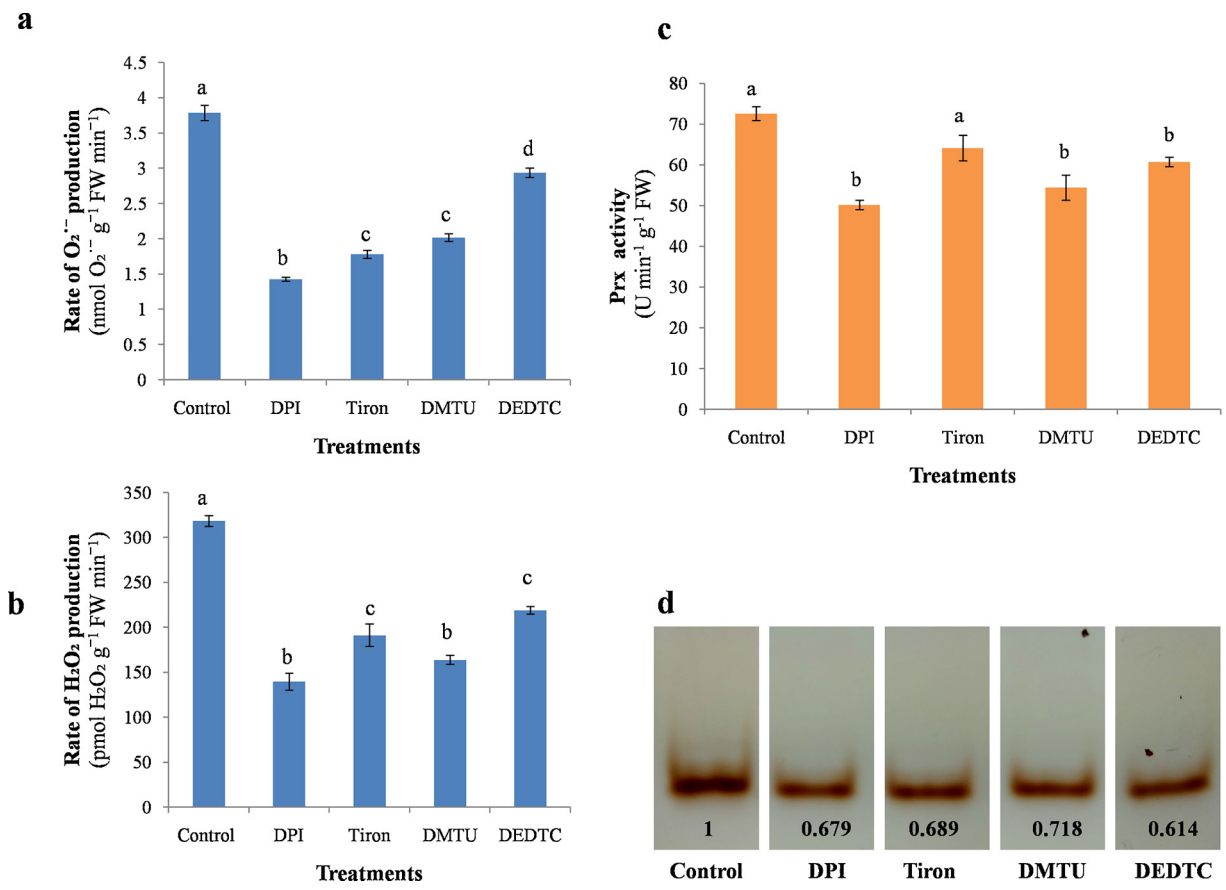


**Fig. 3.** Assay of Prx activity under ROS scavenger and ROS enzyme inhibitor treatment. **(a)** XTT assay of apoplastic $O_2^{\cdot -}$ production by roots of *V. radiata* seedlings grown for 2 days in distilled water (control), DPI (20 μM), Tiron (1 mM), DMTU (1 mM) and DEDTC (1 mM). **(b)** Xylenol orange assay of apoplastic $H_2O_2$ production by roots of seedlings incubated in DPI (20 μM), Tiron (1 mM), DMTU (1 mM) and DEDTC (1 mM) for 2 days along with control values. **(c)** Effects of DPI (20 μM), Tiron (1 mM), DMTU (1 mM) and DEDTC (1 mM) on Prx activity as determined by a spectrophotometric assay ($n = 3$; $F = 15.31$; $p < 0.05$). **(d)** *In-gel* native PAGE assay of Prx using DAB demonstrating the inhibitory effects of DPI (20 μM), Tiron (1 mM), DMTU (1 mM) and DEDTC (1 mM) relative to the control, shown as brown bands. Numeric values denote relative band intensity.

SOD activity was observed at low concentrations (25 μM) while higher concentrations (in the mM range) were significantly inhibitory (Fig. 2c).

### 3.3. Effects of ROS scavengers on Prx

The involvement of ROS in Prx regulation was obvious based on an assessment of Prx activity in extracts from roots treated with ROS enzyme inhibitors and specific ROS scavengers, i.e., DPI (20 μM), Tiron (1 mM), DMTU ($H_2O_2$ scavenger, 1 mM) and DEDTC (SOD inhibitor, 1 mM). As established earlier, root growth in terms of root length and fresh weight was severely inhibited by all the treatment agents (Fig. S2a and b). All of the treatments individually reduced apoplastic superoxide (control: 3.78, DPI: 1.43, Tiron: 1.88, DMTU: 2.02 and DEDTC: 2.94 nmol $g^{-1}$ FW $min^{-1}$) (Fig. 3a) and $H_2O_2$ levels (control: 318.43, DPI: 139.66, Tiron: 191.33, DMTU: 164 and DEDTC: 219 pmol $g^{-1}$ FW $min^{-1}$) (Fig. 3b). Regarding the effects on Prx, spectrophotometric assay results showed a significant inhibition of enzyme activity under individual treatments of DPI (50.22 U $min^{-1}$ $g^{-1}$ FW), DMTU (54.46 U $min^{-1}$ $g^{-1}$ FW), DEDTC (60.82 U $min^{-1}$ $g^{-1}$ FW) and Tiron (64.2 U $min^{-1}$ $g^{-1}$ FW) relative to the control values (72.66 U $min^{-1}$ $g^{-1}$ FW) (Fig. 3c). Native PAGE analysis also demonstrated these inhibitory effects. Considering the intensity of the lowermost band, Prx activity was much less pronounced in the treatment groups than in the control. Although Tiron was less effective in the spectrophotometric assay, its negative influence on Prx was distinct in the PAGE analysis (Fig. 3d).

### 3.4. Effects of $Ca^{+2}$ homeostasis antagonists on SOD and Prx

To explore the potential involvement of $Ca^{+2}$ in controlling SOD and Prx activity, *V. radiata* seedlings (12 h germinated) were incubated in the presence of $LaCl_3$ ($Ca^{+2}$ channel blocker; 100 μM), EGTA ($Ca^{+2}$ chelator; 100 μM) and LiCl (endosomal $Ca^{+2}$ release blocker; 2 mM) (Fig. 4). Root growth was distinctly inhibited by these agents in regard to both the length and fresh weight of root tissue (Fig. S3a and b). Apoplastic superoxide levels were greatly reduced under $LaCl_3$ (2.01 nmol $g^{-1}$ FW $min^{-1}$), LiCl (3.07 nmol $g^{-1}$ FW $min^{-1}$) and EGTA (2.26 nmol $g^{-1}$ FW $min^{-1}$) treatments relative to those of the control (3.98 nmol $g^{-1}$ FW $min^{-1}$). Similarly, $H_2O_2$ production was significantly diminished by $LaCl_3$ (195 pmol $g^{-1}$ FW $min^{-1}$), LiCl (280.33 pmol $g^{-1}$ FW $min^{-1}$) and EGTA (224.33 pmol $g^{-1}$ FW $min^{-1}$) treatments relative to that in the control (318.43 pmol $g^{-1}$ FW $min^{-1}$). Spectrophotometric analysis of SOD activity revealed significant inhibition resulting from treatment with $LaCl_3$ (0.089 U $min^{-1}$ $mg^{-1}$ protein) and EGTA (0.081 U $min^{-1}$ $mg^{-1}$ protein) relative to that in the control (0.111 U $min^{-1}$ $mg^{-1}$ protein), although LiCl (0.103 U $min^{-1}$ $mg^{-1}$ protein) was comparatively less effective and caused only weak inhibition (Fig. 4c). This result was further validated by an in-gel assay, which showed that $LaCl_3$ and EGTA had a strong negative influence on SOD, as the bands corresponding to these treatments were visibly weaker than those observed for the control (Fig. 4d), denoting the need for a threshold $[Ca^{+2}]_{cyt}$ for SOD activity. Like in the spectrophotometric analysis, PAGE analysis demonstrated that LiCl did not affect SOD activity (data not shown). On the other hand, $Ca^{+2}$ appeared

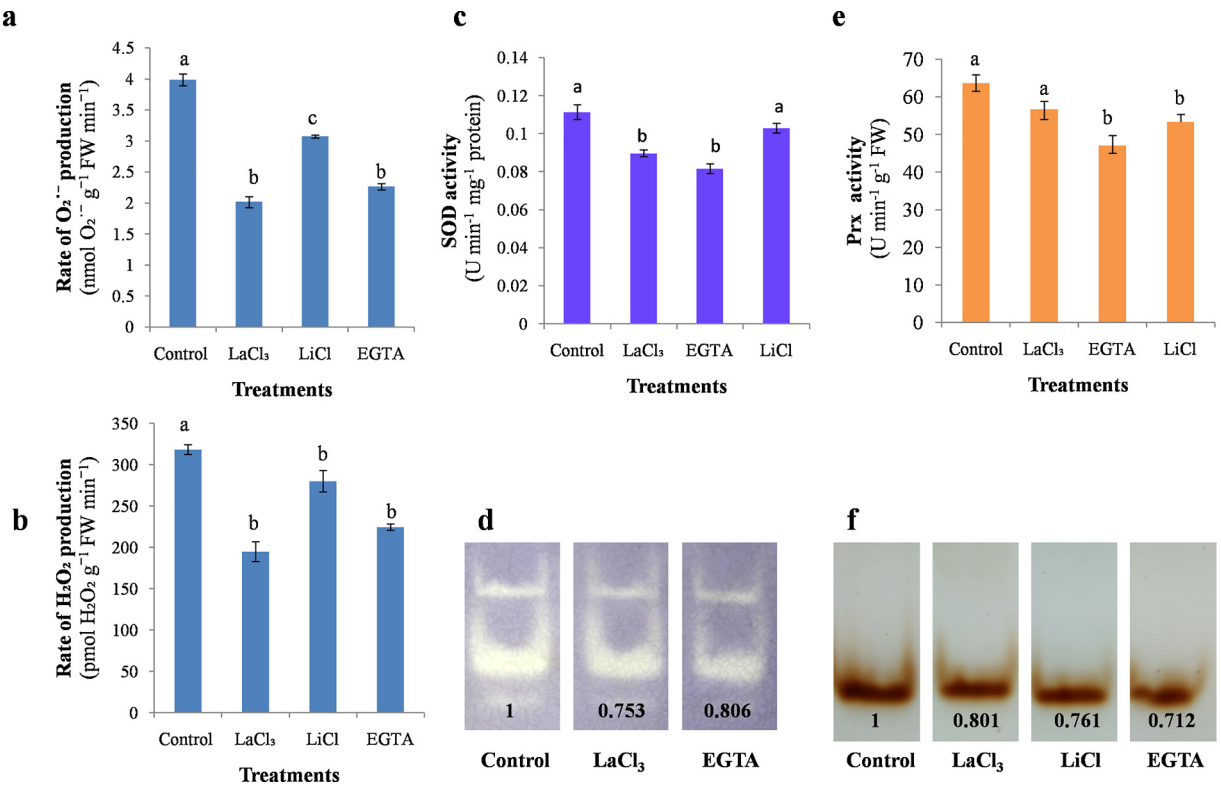


**Fig. 4.** Effects of $Ca^{+2}$ homeostasis antagonists on apoplastic ROS production, SOD activity and Prx activity. **(a)** XTT assay of apoplastic $O_2^{\cdot -}$ production by roots of *V. radiata* seedlings grown for 2 days in distilled water (control), $LaCl_3$ (100 μM), EGTA (100 μM) and LiCl (2 mM). **(b)** Xylenol orange assay of apoplastic $H_2O_2$ production by roots of seedlings incubated in $LaCl_3$ (100 μM), EGTA (100 μM) and LiCl (2 mM) for 2 days along with control values. **(c)** Activity of SOD detected spectrophotometrically in total cellular extracts of roots incubated in $LaCl_3$ (100 μM), EGTA (100 μM) and LiCl (2 mM) along with control values ($n = 3$; $F = 25.92$; $p < 0.05$). **(d)** *In-gel* native PAGE assay of SOD using NBT showing the differential effects of $LaCl_3$ (100 μM), EGTA (100 μM) and LiCl (2 mM) relative to the control, shown as white achromatic bands. Numeric values denote relative band intensity levels. **(e)** Effects of $LaCl_3$ (100 μM), EGTA (100 μM) and LiCl (2 mM) on Prx activity as determined by a spectrophotometric assay ($n = 3$; $F = 9.24$; $p < 0.05$). **(f)** *In-gel* native PAGE assay of Prx derived from DAB demonstrating the inhibitory effects of $LaCl_3$ (100 μM), EGTA (100 μM) and LiCl (2 mM) relative to the control, shown as brown bands. Numeric values denote relative band intensity.

to be involved in Prx regulation, as antagonists considerably modulated Prx activity. Thus, the spectrophotometric assay revealed lower levels of Prx activity in samples treated with EGTA (47.06 U $min^{-1}$ $g^{-1}$ FW) and LiCl (53.3 U $min^{-1}$ $g^{-1}$ FW) than in samples from the control (63.66 U $min^{-1}$ $g^{-1}$ FW). Although $LaCl_3$ (56.65 U $min^{-1}$ $g^{-1}$ FW) reduced Prx activity, the effect was quite mild (Fig. 4e). The same observation was made during native PAGE analysis, which showed that the diminution of Prx was distinct under $LaCl_3$, EGTA and LiCl treatments (Fig. 4f).

### 3.5. Modulation of apoplastic OH radical concentration

The effects of a PM $H^+$-ATPase inhibitor, a ROS enzyme inhibitor, ROS scavengers and $Ca^{+2}$ homeostasis antagonists on Prx activity were further analysed by fluorometrically estimating apoplastic OH radical concentrations (Fig. 5). Corroborating to their inhibitory effects on Prx, both vanadate [A.U. (fluorescence arbitrary unit) 0.133] and CCCP (A.U. 0.126) lowered apoplastic OH levels relative to control levels (A.U. 0.278). ROS scavengers presented diminished OH concentrations (Tiron: A.U. 0.177; DMTU: A.U. 0.178; DEDTC: A.U. 0.144), with DPI (A.U. 0.09) showing the maximum levels of reduction. Similarly, $LaCl_3$, LiCl and EGTA drastically compromised the availability of apoplastic OH (A.U. 0.12, A.U. 0.178 and A.U. 0.111 respectively).

## 4. Discussion

Despite their well-established detrimental effects on living systems, ROS are also known to be involved in diverse aspects of plant physiology, such as responses to environmental stimuli, e.g., chloroplast movement (Majumdar and Kar, 2016), gravitropic bending (Singh et al., 2017), plant growth and development (Causin et al., 2012; Singh et al., 2016; Li et al., 2017), and responses to biotic (O'Brien et al., 2012) and abiotic (Baxter et al., 2013) stress. During root growth, NOX constitutively produces $O_2^-$ by reducing $O_2$ with electrons arising from cytosolic NADPH oxidation (Foreman et al., 2003; Dunand et al., 2007; Fluhr, 2009; Li et al., 2017). However, due to the absence of specific proton channels, such as VSOP/Hv1, in animal phagocytes (Sasaki et al., 2006; Ramsey et al., 2009), NOX activity in plants can form uneven charge distributions across the PM, resulting in membrane depolarization. In our recent report (Majumdar and Kar, 2018), we hypothesized and demonstrated the suitability of PM $H^+$-ATPase as a potent counteracting enzyme by extruding $H^+$ into the apoplast in a coordinated manner. These enzymes are thought to integrate into a positive feed-forward loop based on the observation that a NOX inhibitor and ROS scavengers inhibit PM $H^+$-ATPase while the rates of apoplastic $O_2^-$ production (linked to NOX activity) are greatly reduced during vanadate and CCCP treatment.

However, having a much shorter half-life (2–4 μs) and being impermeable to lipid membranes, NOX-generated apoplastic $O_2^-$ must be rapidly converted into $H_2O_2$, which is more stable, has a longer half-life (1 ms) (Garg and Manchanda, 2009; Černý et al., 2018), can cover distance by diffusion and can cross the PM via aquaporins (Mubarakshina and Ivanov, 2010; Bienert and Chaumont, 2014). Interestingly, the intermediary process of apoplastic $O_2^-$ conversion to $H_2O_2$ appears to be dependent on the cross-PM $H^+$ gradient mediated by PM $H^+$-ATPase, as apoplastic $H_2O_2$ is substantially reduced by vanadate and CCCP treatments (Fig. 1a). As the candidate enzyme responsible for the conversion process, Cu-Zn SOD appears to be

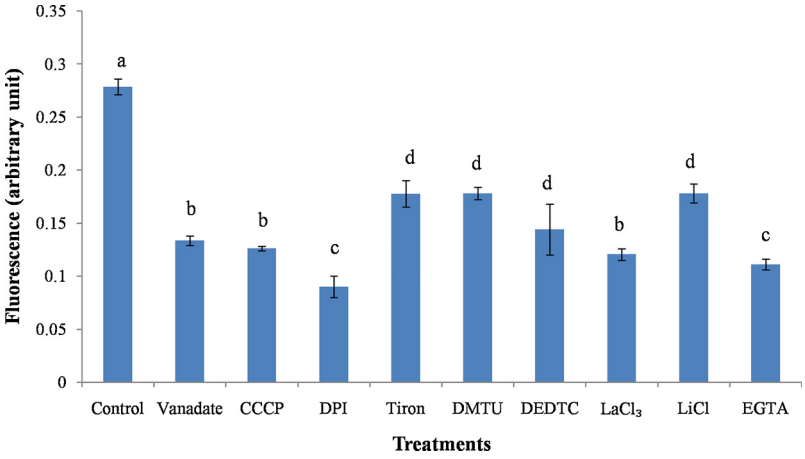


**Fig. 5.** Spectrofluorometric assay of the apoplastic ˙OH radical. Root tissues (400 mg) excised from different treatment groups were incubated in K-phosphate buffer (50 mM, pH 5.8) containing 2.5 mM Na-benzoate for 6 h in the dark on a cyclomixer. After incubation, the fluorescence of the bathing medium was measured (excitation: 305 nm; emission: 407 nm). A rectified value was obtained by subtracting the unspecific fluorescence measured from blanks containing tissue in only buffer (without Na-benzoate).

modulated by treatments that alter $H_2O_2$ production rates. Our observation that both vanadate and CCCP significantly inhibited SOD, as revealed by both spectrophotometric and native PAGE assays (Fig. 1b and c), corroborates this idea. This result implies that PM $H^+$-ATPase effectively influences Cu-Zn SOD activity by regulating the cross-PM extrusion of $H^+$ which serves as a substrate for the latter enzyme. In addition to $H^+$, $O_2^-$ derived from NOX serves as another SOD substrate, and the importance of NOX in regulating SOD activity was demonstrated based on the observation that a NOX inhibitor (DPI) and an $O_2^-$ scavenger (Tiron) significantly inhibited SOD (Fig. 2a and b). Moreover, as PM $H^+$-ATPase and NOX are involved in a feed-forward loop, limiting $H^+$ extrusion inhibits NOX, and a reduction in $O_2^-/H_2O_2$ content depresses PM $H^+$-ATPase (Majumdar and Kar, 2018). These results suggest that the NOX-PM $H^+$-ATPase loop must remain uninhibited for SOD to function properly. The augmentation of SOD activity by $H_2O_2$ at low concentrations (Fig. 2c) can thus be explained by its stimulatory effects on PM $H^+$-ATPase (Li et al., 2011; Majumdar and Kar, 2018) and on inwardly rectifying $Ca^{+2}$ channels, such as HACC (hyperpolarization-activated $Ca^{+2}$ channel) (Demidchik et al., 2002; Foreman et al., 2003; Demidchik, 2018), both of which can induce NOX activity.

The fundamentality of the coordination among the three enzymes (SOD, NOX and PM $H^+$-ATPase) for root growth is supported by growth studies showing drastic reductions in root length and fresh weight upon treatment with vanadate, CCCP (Fig. S1a and b), NOX and SOD inhibitors and different ROS scavengers (Fig. S2a and b). However, as the candidate enzyme responsible for OH formation (necessary for wall loosening resulting in cell growth) from $H_2O_2$ via the hydroxylic cycle (Cosio and Dunand, 2009; Kukavica et al., 2009), class III Prx likely acts as the link between the proposed NOX-ATPase-SOD functional loop and root growth. By modulating the available apoplastic $H_2O_2$ content, the loop is designed to regulate Prx activity via substrate ($H_2O_2$) availability and in turn, growth kinetics. Indeed, our spectrophotometric assay revealed lowered levels of Prx activity (Fig. 1d) during treatment with vanadate and CCCP, which was further confirmed by in-gel assays (Fig. 1e), implying the positive involvement of PM $H^+$-ATPase in Prx activity regulation. The mitigation of Prx activity under DPI, Tiron and DMTU ($H_2O_2$ scavenger) treatments was correlated with a drastic reduction in apoplastic $H_2O_2$ content (Fig. 3). Moreover, when SOD was inhibited by DEDTC treatment, Prx activity was strongly diminished, confirming the importance of SOD as an $H_2O_2$ supplier (Fig. 3). The proposed enzymatic coordination relating to root growth was validated by apoplastic OH estimations. Corroborating their inhibitory effects on Prx, a fluorometric assay showed that the PM $H^+$-ATPase inhibitor, protonophore, ROS enzyme inhibitors, ROS scavengers and $Ca^{+2}$ antagonists significantly reduced apoplastic OH levels (Fig. 5). As Prx is the primary source of apoplastic OH, this observation justifies the hypothesis that Prx is directly influenced by NOX, PM $H^+$-ATPase and apoplastic Cu-Zn SOD.

Interestingly, all of the studied enzymes, i.e., NOX, PM $H^+$-ATPase, SOD and Prx are reportedly dependent on the homeostasis of $Ca^{+2}$ (a potent second messenger; Siddiqui et al., 2012), and root growth was significantly inhibited during treatment with $Ca^{+2}$ antagonists (Fig. S3a and b). While NOX is directly activated by the binding of $Ca^{+2}$ to the N-terminal EF-hand motif, CDPK action, or the $Ca^{+2}$-induced binding of Rho-type GTPase (Sagi and Fluhr, 2006; Ogasawara et al., 2008; Gilroy et al., 2014; Kurusu et al., 2015), PM $H^+$-ATPase is reportedly differentially regulated by $Ca^{+2}$ in a dose-dependent manner (Yu et al., 2006; Janicka-Russak, 2011; Majumdar and Kar, 2018). Thus, the lowering of $O_2^-$ production rates by treatment with $Ca^{+2}$ homeostasis antagonists (Fig. 4a) can be attributed to the potential inhibition of NOX and PM $H^+$-ATPase. In agreement with Choi et al. (2011), the threshold $[Ca^{+2}]_{cyt}$ level required for enzyme activity was found to be dependent on both $Ca^{+2}$ influx via PM (inhibited by $La^{+3}$ and EGTA) and its endosomal release (blocked by Li). $Ca^{+2}$ antagonists likely inhibit Cu-Zn SOD (Fig. 4c and d) by depleting its substrates, i.e., $O_2^-$ and $H^+$, via the upstream inhibition of source enzymes. As a result, the rates of apoplastic $H_2O_2$ production are significantly reduced (Fig. 4b). However, the drop in Prx activity observed (Fig. 4e and f) should not be attributed to only the unavailability of $H_2O_2$ resulting from SOD inactivation. In addition to the role of $Ca^{+2}$ in anchoring Prx to the cell wall (Shah et al., 2004), $Ca^{+2}$ is required for conformational rearrangements of the enzyme from a native state to an active state and thus facilitates its activity (Pintus et al., 2011).

## 5. Conclusion

It can be concluded that in plants, the orchestration of a NOX-PM $H^+$-ATPase positive feedback loop with SOD and Prx activity mediates wall loosening-induced cell growth. Situated immediately downstream from the loop, SOD and Prx are modulated by substrate availability arising from the regulated activity of NOX and PM $H^+$-ATPase. $Ca^{+2}$ influx through the PM and its release from endosomes builds up $[Ca^{+2}]_{cyt}$, which functions as a link for the proposed NOX-PM $H^+$-ATPase-SOD-Prx loop. A working model demonstrating the $Ca^{+2}$-mediated synchronization of enzymes is proposed (Fig. 6).

## Author contributions statement

RKK envisaged the study. AM and RKK designed the work. AM performed the experiments. AM and RKK wrote the article.

## Conflicts of interest

The authors have no conflicts of interest to declare.

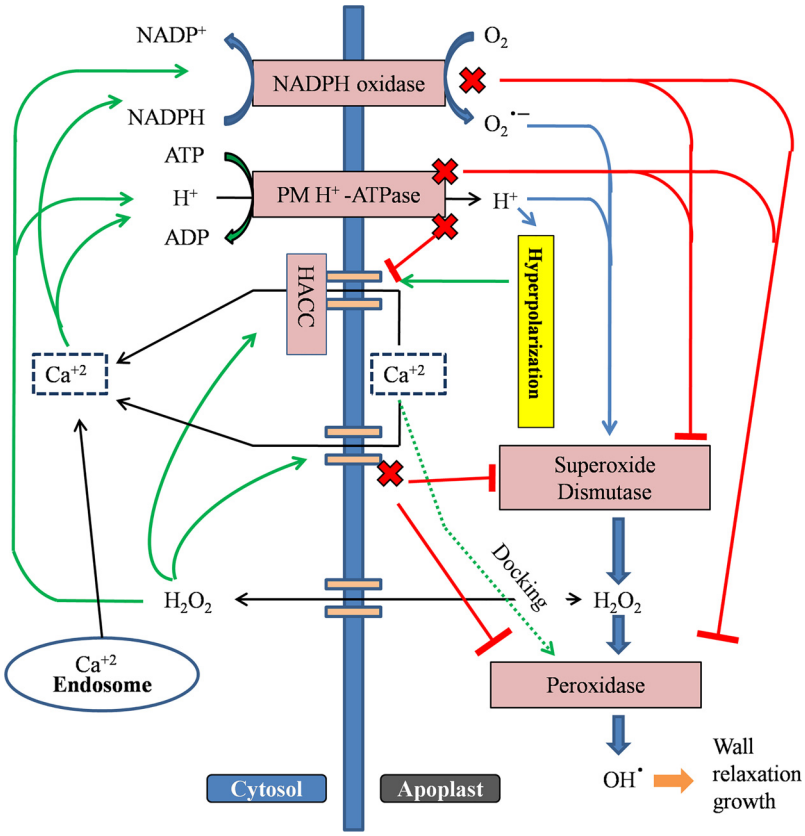


**Fig. 6.** A possible working model demonstrating the $Ca^{+2}$-mediated orchestration of Cu-Zn SOD and class III peroxidase with the upstream interplay of PM $H^+$-ATPase and NADPH oxidase during *Vigna radiata* (L.) Wilczek root growth. As a pre-requisite of cell elongation via wall loosening, PM NADPH oxidase (RBOH) and $H^+$-ATPase remain constitutively active and produce $O_2^{\cdot -}$ and extrude $H^+$ at the apoplast, respectively. Utilizing nascent $O_2^{\cdot -}$ and $H^+$ as substrates, apoplast-located Cu-Zn SOD produces apoplastic $H_2O_2$ via disproportionation reactions. In addition to functioning as a signalling molecule, apoplastic $H_2O_2$ serves as the precursor of the $^{\cdot}OH$ radical required for wall polysaccharide cleavage, which is spurred by the activity of class III peroxidase. HACC (hyperpolarization-activated $Ca^{+2}$ channel) is stimulated by PM $H^+$-ATPase mediated membrane hyperpolarization together with other $H_2O_2$-induced $Ca^{+2}$ channels and by the endosomal release of $Ca^{+2}$ build-up $[Ca^{+2}]_{cyt}$. In addition to activating NOX by directly binding EF-hand motifs and regulating PM $H^+$-ATPase via phosphorylation, $Ca^{+2}$ helps dock Prx at the cell wall and maintain structural integrity and conformational rearrangements. A reduction in apoplastic $^{\cdot}OH$ concentrations and the diminution of SOD and Prx arising from the inhibition of NOX and PM $H^+$-ATPase activity denote their potential integration in an enzymatic complex, in which NOX-ATPase regulates downstream SOD-Prx via controlling substrate availability. Strong negative effects of $Ca^{+2}$ homeostasis antagonists on each of the enzymes denote its potential mediator role.

## Acknowledgements

One author (AM) gratefully recognizes financial support for the current investigation from the University Grants Commission (UGC), New Delhi, India as a BSR fellowship [vide letter F. No. 25-1/2014-15(BSR)/220/2009/(BSR)]. Both authors acknowledge the departmental research facilities created under the UGC-SAP and DST-FIST programmes.

## Appendix A. Supplementary data

Supplementary material related to this article can be found, in the online version, at doi:https://doi.org/10.1016/j.jplph.2018.11.001.

## References

Abedi, T., Pakniyat, H., 2010. Antioxidant enzyme changes in response to drought stress in ten cultivars of oilseed Rape (*Brassica napus* L.). Czech J. Genet. Plant Breed. 46 (1), 27–34.

Airianah, O.B., Vreeburg, R.A.M., Fry, S.C., 2016. Pectic polysaccharides are attacked by hydroxyl radicals in ripening fruit: evidence from a fluorescent fingerprinting method. Ann. Bot. 117, 441–455. https://doi.org/10.1093/aob/mcv192.

Almagro, L., Gómez Ros, L.V., Belchi-Navarro, S., Bru, R., Ros Barceló, A., Pedreño, M.A., 2009. Class III Peroxidases in plant defence reactions. J. Exp. Bot. 60 (2), 377–390. https://doi.org/10.1093/jxb/ern277.

Alscher, R.G., Erturk, N., Heath, L.S., 2002. Role of superoxide dismutases (SODs) in controlling oxidative stress in plants. J. Exp. Bot. 53 (372), 1331–1341.

Baxter, A., Mittler, R., Suzuki, N., 2013. ROS as key players in plant cell signalling. J. Exp. Bot. 65 (5), 1229–1240. https://doi.org/10.1093/jxb/ert375.

Beauchamp, C., Fridovich, I., 1971. Superoxide dismutase: improved assays and an assay applicable to acrylamide gels. Anal. Biochem. 44, 176–187.

Bienert, G.P., Chaumont, F., 2014. Aquaporin-facilitated transmembrane diffusion of hydrogen peroxide. Biochim. Biophys. Acta 1840 (5), 1596–1604. https://doi.org/10.1016/j.bbagen.2013.09.01.

Causin, H.F., Roqueiro, G., Petrillo, E., Lainez, V., Pena, L.B., Marchetti, C.F., Gallego, S.M., Maldonado, S.I., 2012. The control of root growth by reactive oxygen species in *Salix nigra* Marsh. seedlings. Plant Sci. 183, 197–205. https://doi.org/10.1016/j.plantsci.2011.08.012.

Černý, M., Habánová, H., Berka, M., Luklová, M., Brzobohatý, B., 2018. Hydrogen peroxide: its role in plant biology and crosstalk with signalling networks. Int. J. Mol. Sci. 19 (2812), 1–30. https://doi.org/10.3390/ijms19092812.

Chen, C.-N., Pan, S.-M., 1996. Assay of superoxide dismutase activity by combining electrophoresis and densitometry. Bot. Bull. Acad. Sin. 37, 107–111.

Chen, S., Schopfer, P., 1999. Hydroxyl-radical production in physiological reactions. A novel function of peroxidase. Eur. J. Biochem. 260, 726–735.

Choi, W., Swanson, S.J., Gilroy, S., 2011. Coding and decoding of calcium signals in plants. In: Luan, S. (Ed.), Signal Commun Plants. Springer, Berlin, pp. 41–61.

Cosio, C., Dunand, C., 2009. Specific functions of individual class III peroxidase genes. J. Exp. Bot. 60 (2), 391–408. https://doi.org/10.1093/jxb/ern318.

Demidchik, V., 2018. ROS-activated ion channels in plants: biophysical characteristics, physiological functions and molecular nature. Int. J. Mol. Sci. 19 (1263), 1–18. https://doi.org/10.3390/ijms19041263.

Demidchik, V., Bowen, H.C., Maathuis, F.J., Shabala, S.N., Tester, M.A., White, P.J., Davies, J.M., 2002. *Arabidopsis thaliana* root non-selective cation channels mediate calcium uptake and are involved in growth. Plant J. 32, 799–808.

Dunand, C., Crevecoeur, M., Penel, C., 2007. Distribution of superoxide and hydrogen peroxide in Arabidopsis root and their influence on root development: possible interaction with peroxidases. New Phytol. 174, 332–341. https://doi.org/10.1111/j.1469-8137.2007.01995.x.

Fick, G.N., Qualset, C.O., 1975. Genetic control of endosperm amylase activity and gibberellic acid responses in standard-height and short-statured wheats. Proc. Natl. Acad. Sci. U. S. A. 72, 892–895.

Fluhr, R., 2009. Reactive oxygen-generating NADPH oxidases in plants. In: Rio, L.A., Puppo, A. (Eds.), Reactive Oxygen Species in Plant Signalling. Springer-Verlag, Berlin, pp. 1–23.

Foreman, J., Demidchik, V., Bothwell, J.H.F., Mylona, P., Miedema, H., Torres, M.A., Linstead, P., Costa, S., Brownlee, C., Jones, J.D.G., Davies, J.M., Dolan, L., 2003. Reactive oxygen species produced by NADPH oxidase regulate plant cell growth. Nature 422, 442–446.

Francoz, E., Ranocha, P., Nguyen-Kim, H., Jamet, E., Burlat, V., Dunand, C., 2015. Roles of cell wall peroxidises in plant development. Phytochemistry 112, 15–21. https://doi.org/10.1016/j.phytochem.2014.07.020.

Garg, N., Manchanda, G., 2009. ROS generation in plants: boon or bane? Plant Biosyst. 143 (1), 81–96.

Gay, C., Gebicki, J.M., 2000. A critical evaluation of the effect of sorbitol on the ferric-xylenol orange hydroperoxide assay. Anal. Biochem. 284, 217–220.

Giannopolitis, C.N., Ries, S.K., 1977. Superoxide dismutases: occurrence in higher plants. Plant Physiol. 59, 309–314.

Gilroy, S., Suzuki, N., Miller, G., Choi, W.-G., Toyota, M., Devireddy, A.R., Mittler, R., 2014. A tidal wave of signals: calcium and ROS at the forefront of rapid systemic signalling. Trends Plant Sci. 19 (10), 623–630. https://doi.org/10.1016/j.tplants.2014.06.013.

Hager, A., 2003. Role of the plasma membrane $H^+$-ATPase in auxin induced elongation growth: historical and new aspects. J. Plant Res. 116, 483–505.

Janicka-Russak, M., 2011. Plant plasma membrane $H^+$-ATPases in adaptation of plants to

abiotic stresses. In: Shanker, A. (Ed.), Abiotic Stress Response in Plants – Physiological, Biochemical and Genetic Perspectives. InTech, pp. 197–218.
Kar, R.K., 2015. ROS signalling: relevance with site of production and metabolism of ROS. In: Gupta, D.K., Palma, J.M., Corpas, F.J. (Eds.), Reactive Oxygen Species and Oxidative Damage in Plants Under Stress. Springer, Switzerland, pp. 115–125.
Kukavica, B., Mojovic, M., Vucinic, Z., Maksimovic, V., Takahama, U., Jovanovic, S.V., 2009. Generation of hydroxyl radical in isolated Pea root cell wall, and the role of cell wall-bound peroxidase, Mn-SOD and phenolics in their production. Plant Cell Physiol. 50 (2), 304–317. https://doi.org/10.1093/pcp/pcn199.
Kurusu, T., Kuchitsu, K., Tada, Y., 2015. Plant signalling networks involving $Ca^{+2}$ and Rboh/Nox-mediated ROS production under salinity stress. Front. Plant Sci. https://doi.org/10.3389/fpls.2015.00427.
Li, J., Chen, G., Wang, X., Zhang, Y., Jia, H., Bi, Y., 2011. Glucose-6-phosphate dehydrogenase-dependent hydrogen peroxide production is involved in the regulation of plasma membrane $H^+$-ATPase and $Na^+/H^+$ antiporter protein in salt-stressed callus from *Carex moorcroftii*. Physiol. Plant. 141, 239–250. https://doi.org/10.1111/j.1399-3054.2010.01429.x.
Li, W.-Y., Chen, B.-X., Chen, Z.-J., Gao, Y.-T., Chen, Z., Liu, J., 2017. Reactive oxygen species generated by NADPH oxidases promote radicle protrusion and root elongation during rice seed germination. Int. J. Mol. Sci. 18 (110). https://doi.org/10.3390/ijms18010110.
Liszkay, A., Van der Zalm, E., Schopfer, P., 2004. Production of reactive oxygen intermediates ($O_2^-$, $H_2O_2$ and OH) by maize roots and their role in wall loosening and elongation growth. Plant Physiol. 136, 3114–3123.
Majumdar, A., Kar, R.K., 2016. Integrated role of ROS and $Ca^{+2}$ in blue light-induced chloroplast avoidance movement in leaves of *Hydrilla verticillata* (L.f.) Royle. Protoplasma 253 (6), 1529–1539. https://doi.org/10.1007/s00709-015-0911-5.
Majumdar, A., Kar, R.K., 2018. Congruence between PM $H^+$-ATPase and NADPH oxidase during root growth: a necessary probability. Protoplasma 255 (4), 1129–1137. https://doi.org/10.1007/s00709-018-1217-1.
Miller, A.-F., 2003. Superoxide processing. In: Que Jr.L., Tolman, W. (Eds.), Coordination Chemistry in the Biosphere and Geosphere. Pergamon, Oxford, Amsterdam, New York and Tokyo, pp. 479–506.
Miller, A.-F., 2004. Superoxide dismutases: active sites that save, but a protein that kills. Curr. Opin. Chem. Biol. 8, 162–168. https://doi.org/10.1016/j.cbpa.2004.02.011.
Minibayeva, F., Kolesnikov, O., Chasov, A., Beckett, R., Luthje, S., Vylegzhanina, N., Buck, F., Bottger, M., 2009. Wound-induced apoplastic peroxidase activities: their roles in the production and detoxification of reactive oxygen species. Plant Cell Environ. 32 (5), 497–508.
Moothoo-Padayachie, A., Varghese, B., Pammenter, N.W., Govender, P., Sershen, 2016. Germination associated ROS production and glutathione redox capacity in two recalcitrant-seeded species differing in seed longevity. Botany 94 (12), 1103–1114. https://doi.org/10.1139/cjb-2016-0130.
Moural, T.W., Lewis, K.M., Barnaba, C., Zhu, F., Palmer, N.A., Sarath, G., Scully, E.D., Jones, J.P., Sattler, S.E., Kang, C.H., 2017. Characterization of class III peroxidases from Switchgrass. Plant Physiol. 173, 417–433.
Mubarakshina, M.M., Ivanov, B.N., 2010. The production and scavenging of reactive oxygen species in the plastoquinone pool of chloroplast thylakoid membranes. Physiol. Plant. 140, 103–110.
Müller, K., Linkies, A., Vreeburg, R.A.M., Fry, S.C., Krieger-Liszkay, A., Leubner-Metzger, G., 2009. In vivo cell wall loosening by hydroxyl radicals during cress seed germination and elongation growth. Plant Physiol. 150, 1855–1865.
Naderi, R., Valizadeh, M., Toorchi, M., Shakiba, M.R., 2014. Antioxidant enzyme changes in response to osmotic stress in wheat (*Triticum aestivum* L.) seedling. Acta. Biol. Szeged. 58 (2), 95–101.
O'Brien, J.A., Daudi, A., Butt, V.S., Bolwell, G.P., 2012. Reactive oxygen species and their role in plant defence and cell wall metabolism. Planta 236 (3), 765–779. https://doi.org/10.1007/s00425-012-1696-9.
Ogasawara, Y., Kaya, H., Hiraoka, G., Yumoto, F., Kimura, S., Kadota, Y., Hishinuma, H., Senzaki, E., Yamagoe, S., Nagata, K., Nara, M., Suzuki, K., Tanokura, M., Kuchitsu, K., 2008. Synergistic activation of *Arabidopsis* NADPH oxidase AtrbohD by $Ca^{+2}$ and phosphorylation. J. Biol. Chem. 283 (14), 8885–8892. https://doi.org/10.1074/jbc.M708106200.
Ogawa, K., Kanematsu, S., Asada, K., 1997. Generation of superoxide anion and localization of Cu-Zn superoxide sismutase in the vascular tissue of spinach hypocotyls: their association with lignification. Plant Cell Physiol. 38 (10), 1118–1126.
Passardi, F., Cosio, C., Penel, C., Dunand, C., 2005. Peroxidases have more function than a Swiss army knife. Plant Cell Rep. 24, 255–265. https://doi.org/10.1007/s00299-005-0972-6.
Penel, C., Gaspar, T.H., Greppin, H., 1992. Plant Peroxidases, 1980–1990: Topics and Detailed Literature on Molecular, Biochemical, and Physiological Aspects. University of Geneva, Geneva, Switzerland.
Pintus, F., Spano, D., Medda, R., Floris, G., 2011. Calcium ions and a secreted peroxidase in *Euphorbia characias* latex are made for each other. Protein J. 30, 115–123. https://doi.org/10.1007/s10930-011-9310-8.
Prodanovic, O., Prodanovic, R., Bogdanovic, J., Mitrovic, A., Milosavic, N., Radotic, K., 2007. Antioxidative enzymes during germination of two lines of Serbian spruce [*Picea omorika* (Panč.) Purkyně]. Arch. Biol. Sci. 59, 209–216.
Raggi, S., Ferrarini, A., Delledonne, M., Dunand, C., Ranocha, P., Lorenzo, G.D., Cervone, F., Ferrari, S., 2015. The *Arabidopsis* class III peroxidase AtPRX71 negatively regulates growth under physiological conditions and in response to cell wall damage. Plant Physiol. 169, 2513–2525.
Ramsey, I.S., Ruchti, E., Kaczmarek, J.S., Clapham, D.E., 2009. Hv1 proton channels are required for high-level NADPH oxidase-dependent superoxide production during the phagocyte respiratory burst. Proc. Natl. Acad. Sci. U. S. A. 106 (18), 7642–7647. https://doi.org/10.1073/pnas.0902761106.
Rivoal, J., Smith, C.R., Moraes, T.F., Turpin, D.H., Plaxton, W.C., 2002. A method for activity staining after native polyacrylamide gel electrophoresis using a coupled enzyme assay and fluorescence detection: application to the analysis of several glycolytic enzymes. Anal. Biochem. 300, 94–99. https://doi.org/10.1006/abio.2001.5445.
Sagi, M., Fluhr, R., 2006. Production of reactive oxygen species by plant NADPH oxidases. Plant Physiol. 141, 336–340.
Sasaki, M., Takagi, M., Okamura, Y., 2006. A voltage sensor-domain protein is a voltage-gated proton channel. Science 312, 589–592.
Schopfer, P., 1996. Hydrogen peroxide-mediated cell-wall stiffening in vitro in maize coleoptiles. Planta 199, 43–49.
Schopfer, P., 2001. Hydroxyl radical-induced cell-wall loosening *in vitro* and *in vivo*: implications for the control of elongation growth. Plant J. 28 (6), 679–688.
Schopfer, P., Plachy, C., Frahry, G., 2001. Release of reactive oxygen intermediates (superoxide radicals, hydrogen peroxide, and hydroxyl radicals) and peroxidise in germinating radish seeds controlled by light, gibberellins, and abscisic acid. Plant Physiol. 125, 1591–1602.
Shah, K., Penel, C., Gagnon, J., Dunand, C., 2004. Purification and identification of a $Ca^{+2}$-pectate binding POX from *Arabidopsis* leaves. Phytochemistry 65, 307–312.
Siddiqui, M.H., Al-Whaibi, M.H., Sakran, A.M., Basalah, M.O., Ali, H.M., 2012. Effect of calcium and potassium on antioxidant system of *Vicia faba* L. under cadmium stress. Int. J. Mol. Sci. 13, 6604–6619. https://doi.org/10.3390/ijms13066604.
Singh, K.L., Chaudhuri, A., Kar, R.K., 2015. Role of peroxidase activity and $Ca^{+2}$ in axis growth during seed germination. Planta 242 (4), 997–1007. https://doi.org/10.1007/s00425-015-2338-9.
Singh, R., Singh, S., Parihar, P., Mishra, R.K., Tripathi, D.K., Singh, V.P., Chauhan, D.K., Prasad, S.M., 2016. Reactive oxygen species (ROS): beneficial companions of plants' developmental processes. Front. Plant Sci. 7, 1299. https://doi.org/10.3389/fpls.2016.01299.
Singh, K.L., Mukherjee, A., Kar, R.K., 2017. Early axis growth during seed germination is gravitropic and mediated by ROS and calcium. J. Plant Physiol. 216, 181–187.
Tsukagoshi, H., 2016. Control of root growth and development by reactive oxygen species. Curr. Opin. Plant Biol. 29, 57–63. https://doi.org/10.1016/j.pbi.2015.09.008.
Woith, E.W., Stintzing, F., Melzig, M.F., 2017. SOD activity and extremophilicity: a screening of various plant species. Pharmazie 72, 490–496. https://doi.org/10.1691/ph.2017.7493.
Yu, X.-C., Li, M.-J., Gao, G.-F., Feng, H.-Z., Geng, X.-Q., Peng, C.-C., Zhu, S.-Y., Wang, X.-J., Shen, Y.-Y., Zhang, D.-P., 2006. Abscisic acid stimulates a calcium-dependent protein kinase in grape berry. Plant Physiol. 140, 558–579. https://doi.org/10.1104/pp.105.074971.